Electron Excitation Functions of Mercury*

RICHARD J. ANDERSON,† EDWARD T. P. LEE, AND CHUN C. LIN‡
Department of Physics, University of Oklahoma, Norman, Oklahoma
(Received 10 October 1966)

Absolute excitation functions of some 40 transitions of the mercury atom have been measured. As in the case of helium, the excitation functions of the singlet states have the common feature of a broad maximum around 30 eV, whereas the triplet states show the characteristic sharp peaks at lower voltages. The excitation functions of the lower states exhibit fine structure near the threshold, which may be attributed to cascade from the states of higher energies. The cascading effect has been examined for the excitation of the $7\,^1S_0$, $7\,^3S_1$, $7\,^3P_2$, $6\,^3D_3$, and $6\,^3D_2$ states. At 15 eV the cascade corrections are small for $7\,^3P_2$, $6\,^3D_3$, and $6\,^3D_2$, but amount to approximately 42% for $7\,^1S_0$. The major source of population of the $7\,^3S_1$ state is found to be cascade transitions from the $7\,^3P_2$ state rather than direct excitation. Direct-excitation cross sections of the $7\,^1S_0$, $6\,^3D_2$, $6\,^3D_3$, and $7\,^3P_2$ states at 15 eV have been determined and the results are compared with the theoretical calculations.

I. INTRODUCTION

RECENT studies of the electron excitation of helium have revealed many interesting aspects of the collisional-excitation processes. The excitation cross sections of the triplet states are found to be much larger than the theoretical values, leading to the conclusion that the population of the triplet states is produced primarily by indirect processes.[1] The pressure dependence of the cross section of the $3\,^3D$ state at 100 eV was ascribed to the $n\,^1P$–nF collisional transfer followed by cascade transitions to the $3\,^3D$ state.[2–4] This explanation was further confirmed by the measurements of the lifetime of the excited states[5–7] and by the excitation-transfer experiments of Robertson *et al.*[8,9]

To further the study of the excitation processes of atoms we have undertaken a detailed investigation of the electron excitation of mercury, which was chosen because it is structurally similar to helium and is readily available in a gaseous phase. The mixing of the singlet and triplet states which is responsible for the intercombination lines adds some interesting features to the excitation functions. We have determined the optical excitation functions for some 40 lines of mercury from which the general shapes of the excitation functions for the various states are established. A cascade analysis is carried out for the $7\,^1S_0$, $7\,^3P_2$, $6\,^3D_3$, $6\,^3D_2$ states, and the direct excitation cross sections of these states are compared with the theoretical calculations.

II. EXPERIMENT

The apparatus involves three basic components: (1) an evacuated excitation tube with a source of mercury atoms, (2) an electron gun to provide a constant flux of electrons into a field-free collision region, and (3) auxiliary equipment to detect and record the radiation emitted as the excited atoms return to states of lower energy. A block diagram of the apparatus is displayed in Fig. 1. The source of ground-state atoms consisted of a small mercury droplet placed in a thermally regulated appendage of the excitation tube. The tube was sealed off from the vacuum system and the atom-number density was estimated from the saturated vapor pressure data of Ernsberger and Pitman.[10]

The electron beam was produced by an oxide-coated cathode, and directed into the collision region by an electron gun of pentode design as shown in Fig. 2. The electron flux is kept constant over the range of 5 to 100 eV by a degenerative feedback system in which the collision chamber current is sampled by a current sensor.

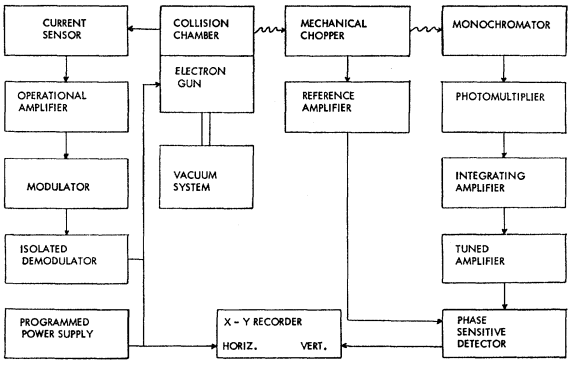

FIG. 1. Block diagram of the experimental apparatus.

* Supported by the U. S. Air Force Weapons Laboratory, Kirtland Air Force Base, New Mexico, a part of the Research and Technology Division of the Air Force System Command, under Contract No. AF 29(601)-6020, and by the U. S. Office of Scientific Research.

† Present address: Department of Physics, University of Arkansas, Fayetteville, Arkansas.

‡ Alfred P. Sloan Foundation Fellow.

[1] R. M. St. John, F. L. Miller, and C. C. Lin, Phys. Rev. **134**, A888 (1964).

[2] R. M. St. John and R. G. Fowler, Phys. Rev. **122**, 1813 (1961).

[3] C. C. Lin and R. G. Fowler, Ann. Phys. (N.Y.) **15**, 461 (1961).

[4] C. C. Lin and R. M. St. John, Phys. Rev. **128**, 1749 (1962).

[5] R. G. Fowler, T. M. Holtzberlein, C. H. Jacobson, and S. J. B. Corrigan, Proc. Phys. Soc. (London) **84**, 539 (1964).

[6] W. R. Pendleton and R. H. Hughes, Phys. Rev. **138**, A683 (1965).

[7] R. B. Kay and R. H. Hughes, Phys. Rev. **154**, 61 (1967).

[8] M. P. Teter, F. E. Niles, and W. W. Robertson, J. Chem. Phys. **44**, 3018 (1966).

[9] M. P. Teter and W. W. Robertson, J. Chem. Phys. **45**, 2167 (1966).

[10] F. M. Ernsberger and H. W. Pitman, Rev. Sci. Instr. **26**, 584 (1955).

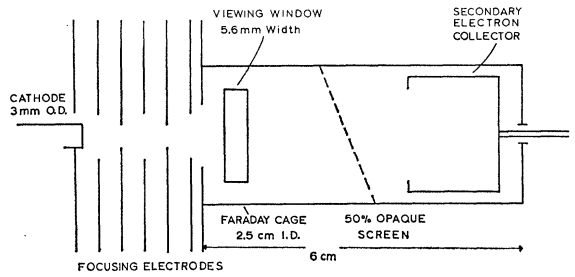

FIG. 2. Schematic diagram of the excitation tube. The spacings between adjacent grids are about 2 mm.

When the electron current exceeds the desired level, a current comparator converts the difference into a voltage signal, which is amplified by an operational amplifier. The cathode is referenced to a variable negative potential; therefore, for the purpose of isolation the control signal is used to modulate a carrier. The modulated signal is amplified, demodulated, and applied to the first grid. Its application results in a change of the voltage-current characteristics of the excitation tube. Thus, if the potentials of the first two grids are properly chosen the beam current will be decreased to the desired value. The third electrode is held at cathode potential while the remaining grids and the Faraday cage are held at ground potential. In this manner, the energy of the electron beam entering the collision chamber is determined solely by the negative potential applied to the cathode. The current stability of the system is better than 0.5%, with an electron energy spread within the range of 0.4 to 0.8 eV. The latter is determined by the appearance of fine structure in the $7\,^3S_1$–$6\,^3P_2$ excitation function and retarding potential measurements. As a test for possible distortions of the electron beam due to instrumentation, the excitation functions of some selected transitions were measured at different beam currents. The excitation functions of a given line taken at different currents do indeed have the same shape and their magnitudes are in proportion to the beam currents.

The radiation produced by the excited atoms is modulated at a frequency of 1 kc/sec. The detection system (tuned amplifier and phase-sensitive detector) for the photomultiplier output is similar to that described by St. John *et al.*[11] However, it is no longer necessary to divide the photomultiplier current by the electron beam current since the latter is maintained at a constant level.

The method used to obtain absolute measurements of the excitation cross sections has been described by St. John *et al.*[1] Measurements of the cross sections of the transitions $7\,^3P_2$–$7\,^3S_1$ (11 287 Å) and $7\,^1S_0$–$7\,^1P_1$ (10 140 Å) were obtained by replacing the photomultiplier detector with type I-Z Kodak spectroscopic plate. The type I-Z emulsion was hypersensitized in order to extend its spectral sensitivity to 12 000 Å. Adjacent portions of the plate were exposed for equal periods of time by the ribbon lamp and the excitation tube. The values of the emissivity of tungsten at 1200°K were obtained by extrapolating the emissivity data of DeVos.[12] The plate was processed immediately after its exposure and the photographic density of the two images was determined to yield an intensity comparison of the two sources.

[11] R. M. St. John, C. C. Lin, R. L. Stanton, H. D. West, J. P. Sweeney, and E. A. Rinehart, Rev. Sci. Instr. **33**, 1089 (1962).

III. THEORY

The mercury atom is treated as a two-electron system. The Hartree-Fock wave functions for the $6s$, $6p$, $6d$, and $7s$ states have been computed by Mishra.[13] These atomic orbitals are used to construct the basis functions of the two-electron system in the $LSJM_J$ representation for each configuration. The spin-orbit interaction which is approximated by

$$\sum_{i=1,2} \xi_i(r)\mathbf{l}_i\cdot\mathbf{s}_i, \tag{1}$$

causes a mixing between states of the same L, J, M_J but different S. The wave functions for the $^1P_1$ and $^3P_1$ states should be written as

$$\begin{aligned}\Psi(^1P_1)&=\alpha\psi(^1P_1)+\beta\psi(^3P_1),\\ \Psi(^3P_1)&=-\beta\psi(^1P_1)+\alpha\psi(^3P_1),\end{aligned} \tag{2}$$

and the same applies to the $^1D_2$ and $^3D_2$ states. The wave functions for the other states are simply taken as the $LSJM_J$ eigenfunctions of a single configuration. For the P states the mixing coefficients can be determined from their fine structure. Here one uses the experimental values of the three energy spacings between the $n\,^1P_1$ and $n\,^3P_{2,1,0}$ levels to determine parametrically the exchange integrals $K_{6s,np}$ and the spin-orbit coupling constants λ_{np}, from which the mixing coefficients can be obtained. Because of the approximate nature of the theory, a reasonably satisfactory fit of the three fine-structure spacings can be achieved by employing a range of values for K and for λ. The mixing coefficient so obtained for the $(6s)(6p)$ configuration is $\beta=0.16\pm0.04$. Alternatively, one can determine the mixing coefficient from the experimental g factor. Lurio[14] gave $\beta=0.1725$, in good agreement with the value derived from the measurements of the lifetime[14] of the $6\,^1P_1$ state ($\beta=0.1714$). For the $(6s)(7p)$ states, we get $\beta=0.54\pm0.08$ from fine-structure energies, but no g factor or lifetime data are available.

The D states are in contradiction with the theory outlined above in that experimental observation shows the ^1D level lying below the ^3D. This discrepancy could be due to the neglect of configuration interaction and spin-other-orbit interaction in the present approxi-

[12] J. C. DeVos, Physica **20**, 715 (1954).
[13] B. Mishra, Proc. Cambridge Phil. Soc. **48**, 511 (1952).
[14] A. Lurio, Phys. Rev. **140**, A1505 (1965).

mation. Wolfe[15] has included the spin-other-orbit interaction in the Hamiltonian for the fine structure. It is possible to use Wolfe's formulas which contain an additional parameter of the spin-other-orbit coupling constant, to fit the fine-structure energy levels and obtain β.[16] However, it is not clear that one can ascribe the "anomalous" inversion of the ^1D and ^3D states completely to the spin-other-orbit interaction. In fact, it has been shown that configuration interaction alone may also produce such an inversion.[17] Results derived from fitting three experimental numbers to three parameters may not have much theoretical significance. Therefore, we prefer to use the g factor to find the mixing coefficient. For the $6\,^1D_2$ state, we get $\beta=0.58\pm0.02$ from the data of Van Kleef and Fred.[18] The error limit given here is that associated with the experimental errors of the measurements. The value of β may be subject to a larger uncertainty because of the approximate nature of the theoretical model used.

Table I lists the transition probabilities of 17 transitions which were used to evaluate the apparent excitation cross sections from the optical-excitation data. The dipole matrix elements are calculated using Mishra's self-consistent field wave functions. The transition probabilities for some of the intercombination lines are subject to rather large uncertainties because of the inaccuracy of the singlet-triplet mixing coefficients.

The direct excitation function of the $7\,^1S_0$ state was calculated by the Born approximation. For the P and D states which contain both singlet and triplet character, the Born approximation was used for the components of the transition integrals corresponding to singlet-singlet transitions while the singlet-triplet components were evaluated by the Born-Oppenheimer approximation. The reason for employing such a mixed scheme of calculation is that for excitations which do not involve change of spin multiplicity, the Born approximation is believed to be more reliable than the Born-Oppenheimer one.[19] Recently, Ochkur[20] has suggested a simplified method for calculating cross sections of exchange excitation. For comparison we have also included cross sections computed by Ochkur's method in lieu of the Born-Oppenheimer approximation. The results of the theoretical calculations for the $7\,^1S_0$, $7\,^3P_2$, $6\,^3D_3$, and $6\,^3D_2$ states are summarized in Fig. 3. Since the excitation cross sections of the singlet states are much larger than the corresponding triplet states, the calculated cross section of the $6\,^3D_2$ state owes its origin to the singlet component of the mixed wave function and is therefore very sensitive to the magnitude of the mixing coefficients.

TABLE I. Transition probabilities (in units of 10^8 sec^{-1}).[a]

Transition	$A(j,k)$	Transition	$A(j,k)$
$7\,^3P_2$–$7\,^3S_1$	0.44	$7\,^3S_1$–$6\,^3P_2$	1.1
$7\,^3P_1$–$7\,^3S_1$	0.18	$7\,^3S_1$–$6\,^3P_1$	1.2
$7\,^3P_0$–$7\,^3S_1$	0.23	$7\,^3S_1$–$6\,^3P_0$	0.52
$7\,^3P_1$–$7\,^1S_0$	0.035±0.004	$7\,^3S_1$–$6\,^1P_1$	0.002
$7\,^1P_1$–$7\,^1S_0$	0.18 ±0.05	$7\,^1S_0$–$6\,^1P_1$	0.29
$7\,^1P_1$–$7\,^3S_1$	0.15 ±0.04	$7\,^1S_0$–$6\,^3P_1$	0.13
$7\,^3P_1$–$6\,^1S_0$	0.13 ±0.03	$6\,^3D_2$–$6\,^3P_2$	0.54±0.02
$7\,^1P_1$–$6\,^1S_0$	0.37 ±0.04	$6\,^3D_2$–$6\,^3P_1$	3.3 ±0.1
		$6\,^3D_2$–$6\,^1P_1$	0.16±0.02

[a] The mixing coefficients used for calculating the transition probabilities are $\beta=0.172\pm0.001$, 0.54 ± 0.08, 0.58 ± 0.02 for the $6P$, $7P$, $6D$ states, respectively. The limits of uncertainty assigned to the values of $A(j,k)$ were derived from those of the mixing coefficients but do not include the errors due to the inaccuracy of the radial wave functions.

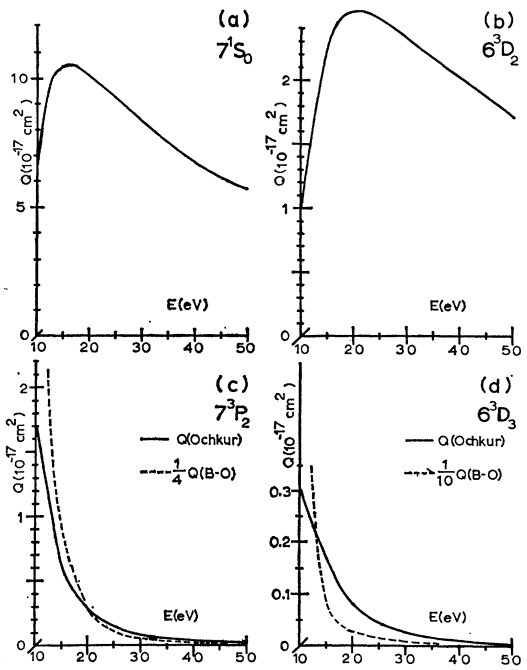

FIG. 3. Theoretical excitation functions (direct) of the $7\,^1S_0$, $6\,^3D_2$, $6\,^3D_3$, and $7\,^3P_2$ states. Curves (c) and (d) give the values calculated by the Born-Oppenheimer approximation and by Ochkur's method. The excitation cross sections for the $6\,^3D_2$ state were calculated by using $\beta=0.58$.

IV. EXPERIMENTAL RESULTS

The excitation functions of some 40 lines of mercury have been measured from 0 to 80 eV. The measurements were carried out for electron beam currents within the range of 10 to 100 μA and at gas densities corresponding to the pressure range 8×10^{-4} to 1×10^{-3} Torr. A detailed investigation of the light output as a function of beam current and gas density was carried out for transitions eminating from the $7\,^3S_1$, $7\,^1S_0$, and $8\,^1P_1$

[15] H. Wolfe, Phys. Rev. **41**, 443 (1932).
[16] R. I. Semenov and B. A. Strugach, Opt. i Spektroskopiya **18**, 756 (1965) [English transl.: Opt. Spectry. (USSR) **18**, 428 (1965)].
[17] R. F. Bacher, Phys. Rev. **43**, 264 (1933).
[18] Th. A. M. Van Kleef and M. Fred, Physica **29**, 389 (1963).
[19] D. R. Bates, A. Fundaminsky, and H. S. W. Massey, Phil. Trans. Roy. Soc. (London) **A243**, 93 (1950).
[20] V. I. Ochkur, Zh. Eksperim. i Teor. Fiz. **45**, 734 (1963) [English transl.: Soviet Phys.—JETP **18**, 503 (1964)].

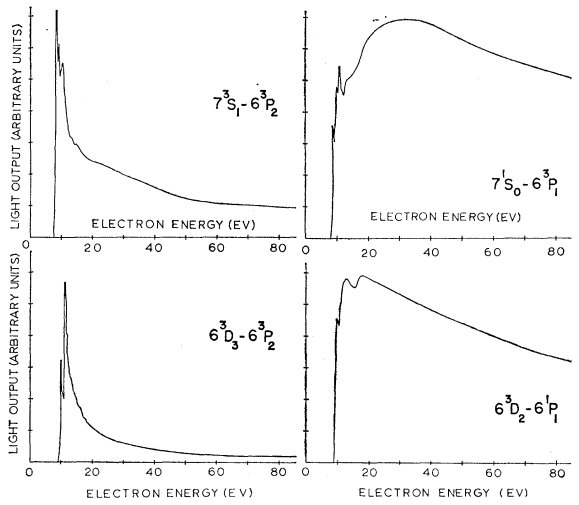

FIG. 4. Optical excitation functions of the "primary" transitions.

levels. Both relationships were observed to be linear for currents up to 200 μA and gas pressures up to 1.2×10^{-3} Torr. The excitation cross sections at 15 eV and at 50 eV are listed in Table II. Figure 4 shows the excitation functions of the 4078 Å ($7\,^1S_0$–$6\,^3P_1$), 5461 Å ($7\,^3S_1$–$6\,^3P_2$), 5770 Å ($6\,^3D_2$–$6\,^1P_1$), and 3650 Å ($6\,^3D_3$–$6\,^3P_2$) transitions. We shall refer to these lines as the "primary" lines for they are used to determine the apparent excitation cross sections of the $7\,^1S_0$, $7\,^3S_1$, $6\,^3D_2$, and $6\,^3D_3$ states. The optical excitation data for all the other lines (called the "secondary" lines) serve chiefly to provide the cascade corrections to the excitation cross sections of the above-mentioned states. Typical examples of the excitation functions of the "secondary" lines are displayed in Fig. 5. It was observed that the experimental onset potentials were consistently larger than the corresponding theoretical values. This discrepancy appeared to be constant for all of the curves obtained and correspond to an energy difference of approximately 2±0.5 eV. The causes of this effect are discussed in detail by Jongurius.[21] This effect has been counteracted by adjusting each of the curves so that the experimental and theoretical onset potentials coincide.

For many of the transitions listed in Table II, adjacent lines of Hg II and in some cases of Hg I are present within a few angstroms. Complete resolution of the observed transitions is possible for only about 30% of the excitation functions. The transitions which do not involve very large quantum numbers are generally expected to be of sufficiently greater intensity than the adjacent lines, hence the observed excitation functions are not appreciably altered by the contamination. In the case of many of the weaker lines, it was necessary to increase the slit width of the monochromator to obtain sufficient intensities. Their excitation functions may then be distorted considerably by the lines of the ionized mercury spectrum and even lines corresponding to Hg I transitions. The lowest possible excited state for the Hg II lines has an onset potential of approximately 17 eV. The excitation functions of seven Hg II transitions have been observed by Schaffernicht[22] to possess a broad maximum occuring at either 55 or 90 eV. Therefore, one would expect little distortion of the observed excitation functions due to the Hg II lines below 20 eV.

The relative shapes of the optical excitation functions displayed in Figs. 4 and 5 exhibit good agreement with those reported by Jongerius,[21] by Schaffernicht,[22] and

TABLE II. Observed values of optical excitation cross sections.

Transition	Wavelength (Å)	$Q(j,k)$ in 10^{-19} cm² at 15 eV	at 50 eV
$8\,^1P_1$–$7\,^1S_0$	6716	9.2 ±1.3	21±3
$9\,^1P_1$–$7\,^1S_0$	6234	6.5 ±1.2	10±1.3
$10\,^1P_1$–$7\,^1S_0$	5803	0.83±0.17	1.6 ±0.2
$11\,^1P_1$–$7\,^1S_0$	5549	0.43±0.08	0.54±0.11
$12\,^1P_1$–$7\,^1S_0$	5393	0.27±0.04	0.62±0.10
$13\,^1P_1$–$7\,^1S_0$	5290	0.25±0.06	0.14±0.05
$14\,^1P_1$–$7\,^1S_0$	5219	0.15±0.04	0.18±0.05
$8\,^1P_1$–$7\,^3S_1$	6072	5.4 ±0.8	7.2 ±0.9
$9\,^1P_1$–$7\,^3S_1$	5676	4.3 ±0.7	6.8 ±1.0
$10\,^1P_1$–$7\,^3S_1$	5317	1.3 ±0.2	0.72±0.10
$11\,^1P_1$–$7\,^3S_1$	5102	0.13±0.03	0.59±0.12
$12\,^1P_1$–$7\,^3S_1$	4970	0.14±0.03	0.14±0.03
$13\,^1P_1$–$7\,^3S_1$	4883	0.19±0.04	0.52±0.11
$14\,^1P_1$–$7\,^3S_1$	4822	0.16±0.04	0.11±0.03
$7\,^3P_2$–$7\,^3S_1$	11287	250±80	
$8\,^3P_2$–$7\,^3S_1$	6907	4.1 ±0.6	1.2 ±0.2
$9\,^3P_2$–$7\,^3S_1$	5821	0.34±0.08	0.19±0.04
$9\,^3P_1$–$7\,^3S_1$	5859	0.44±0.08	0.57±0.11
$9\,^3P_0$–$7\,^3S_1$	5872	0.31±0.07	0.73±0.19
$10\,^3P_2$–$7\,^3S_1$	5354	0.40±0.08	0.16±0.04
$10\,^3P_{1,0}$–$7\,^3S_1$	5385-89	0.09±0.02	0.22±0.05
$11\,^3P_2$–$7\,^3S_1$	5121	0.39±0.06	0.24±0.05
$11\,^3P_{1,0}$–$7\,^3S_1$	5138-40	0.21±0.05	0.17±0.04
$12\,^3P_2$–$7\,^3S_1$	4981	0.30±0.07	0.12±0.03
$12\,^3P_1$–$7\,^3S_1$	4992	0.21±0.05	0.10±0.03
$13\,^3P_{2,1}$–$7\,^3S_1$	4890-97	0.16±0.04	0.32±0.08
$14\,^3P_{2,1}$–$7\,^3S_1$	4827-32	0.18±0.04	0.13±0.03
$7\,^1S_0$–$6\,^1P_1$	10140	64±13	
$8\,^1S_0$–$6\,^1P_1$	4916	11±1.5	17±2
$9\,^1S_0$–$6\,^1P_1$	4108	2.7 ±0.3	4.5 ±0.6
$10\,^1S_0$–$6\,^1P_1$	3802	0.72±0.11	0.24±0.04
$7\,^1S_0$–$6\,^3P_1$	4078	13±1.5	15±2
$8\,^3S_1$–$6\,^1P_1$	5025	0.15±0.06	0.11±0.05
$9\,^3S_1$–$6\,^1P_1$	4140	0.10±0.03	0.16±0.05
$10\,^3S_1$–$6\,^1P_1$	3816	0.13±0.05	0.26±0.08
$7\,^3S_1$–$6\,^3P_2$	5461	70±8	30±3
$7\,^3S_1$–$6\,^3P_1$	4358	59±6	25±3
$7\,^3S_1$–$6\,^3P_0$	4047	19±2	8.2 ±0.9
$6\,^3D_1$, $6\,^1D_2$ –$6\,^1P_1$	5790-91	42±5	34±4
$6\,^3D_2$ –$6\,^1P_1$	5770	28±3	22±3
$7\,^3D_2$, $7\,^1D_2$ –$6\,^1P_1$	4343-47	18±3	20±3
$8\,^3D_{2,1}$, $8\,^1D_2$ –$6\,^1P_1$	3901-03-06	4.8 ±0.8	7.4 ±1.2
$9\,^3D_{2,1}$, $9\,^1D_2$ –$6\,^1P_1$	3701-02-04	1.2 ±0.2	1.7 ±0.3
$6\,^3D_3$–$6\,^3P_2$	3650	75±3	12±2
$6\,^3D_2$–$6\,^3P_2$	3655	5.9 ±1.2	6.8 ±1.1
$6\,^3D_1$, $6\,^1D_2$ –$6\,^3P_2$	3663	5.7 ±1.0	5.1 ±1.0

[21] J. A. Smit and H. M. Jongerius, Appl. Sci. Res. **B5**, 59 (1956); H. M. Jongerius, dissertation, University of Utrecht, 1961 (unpublished).

[22] W. Schaffernicht, Z. Physik **62**, 106 (1930).

by Frisch and Zapesochny.[23] The excitation functions reported by Jongerius were limited to the energy range 0–20 eV, while those of Schaffernicht and Zapesochny extended the range up to 70 eV. Schaffernicht's results did not possess the fine structure observed by Jongerius and by Frisch and Zapesochny. The appearance of such structure near the onset of the excitation function is related to the energy distribution of the electron beam. Employing an extremely univelocity electron beam ($\Delta E = 0.08$ eV), Zapesochny and Shpenik[24] have recently increased the resolution of the fine structure appearing in the $7\,^3S_1$–$6\,^3P_2$ excitation function. The improved technique has only been applied to the most intense transitions of the mercury and helium spectra. The energy distribution of the electron beam used in the present investigation is comparable to that obtained by Jongerius and the earlier work of Zapesochny. The increased sensitivity of the detection apparatus permitted the observation of a number of previously unattainable excitation functions.

Absolute cross sections have been measured by Hanle and Schaffernicht[25] for eight transitions of the visible mercury spectrum at 60 eV. Thieme[26] carried out relative cross sections for additional lines and normalized his data to the absolute value of the $7\,^3S_1$–$6\,^3P_1$ cross section reported by Hanle and Schaffernicht. More recent absolute measurements were made by Jongerius.[21] A comparison of our data with those of the previous works is given in Table III. The measurements are

TABLE III. Comparison of optical excitation cross sections. (All cross sections are expressed in units of 10^{-19} cm^2.)

Transition	$Q(j,k)$ at 15 eV This work	Jongerius	$Q(j,k)$ at 60 eV This work	Hanle-Schaffernicht	Thieme
$7\,^3S_1$–$6\,^3P_2$	70±7	45±5	25±3	67	57
$7\,^3S_1$–$6\,^3P_1$	59±6	36±4	21±2	82	···
$7\,^3S_1$–$6\,^3P_0$	19±2	13±1.3	6.8±0.7	38	31
$7\,^1S_0$–$6\,^3P_1$	13±1.5	9.6±1	14±2	···	56
$8\,^1S_0$–$6\,^1P_1$	11±1.5	8.4±0.9	16±2	···	20
$9\,^1S_0$–$6\,^1P_1$	2.7±0.3	2.0±0.25	4.1±0.5	···	94
$8\,^1P_1$–$7\,^3S_1$	5.4±0.8	···	7.0±1	···	18
$9\,^1P_1$–$7\,^3S_1$	4.3±0.7	3.0±0.4	6.9±1	···	18
$6\,^3D_3$–$6\,^3P_2$	75±13	78±9	9.5±1.7	13	···
$6\,^3D_2$–$6\,^1P_1$	28±3	24±3	20±3	52	58
$9\,^1P_1$–$7\,^1S_0$	6.5±1.2	···	10±2	···	25
$6\,^1D_2$, $6\,^3D_1$ –$6\,^1P_1$	42±5	36±4	30±4	105	92
$6\,^3D_1$, $6\,^1D_2$ –$6\,^3P_2$	5.7±1	6.3±1.2	4.6±0.9	···	···

[23] S. Frisch, Spectrochim. Acta **11**, 350 (1957); I. P. Zapesochny, Vestn. Leningr. Univ., Ser. Fiz. i Khim. **9**, 67 (1954).
[24] I. P. Zapesochny and O. B. Shpenik, in *Proceedings of the Fourth International Conference on the Physics of Electronic and Atomic Collisions* (Science Bookcrafters, Inc., Hastings-on-Hudson, New York, 1965), p. 391.
[25] W. Hanle and W. Schaffernicht, Ann. Physik **6**, 905 (1930).
[26] O. Thieme, Z. Physik **78**, 412 (1932).

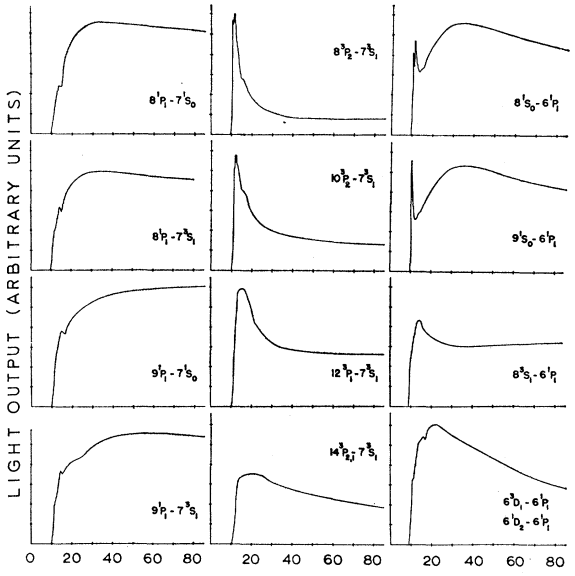

FIG. 5. Typical optical excitation functions of 12 mercury levels. Electron energy ranges from 0 to 80 eV.

compared at the electron energies reported by the authors. The measurements of Hanle and Schaffernicht and of Thieme are about two to four times larger than those of the present work. It is interesting to note that Thieme's excitation cross-section measurements for helium which are also based on Hanle's absolute measurement exhibit serious disagreement with the more recent experiments.[1] On the other hand, our absolute cross sections are consistently larger, with the exception of the $6\,^{3,1}D_2$–$6\,^3P_2$ and $6\,^3D_3$–$6\,^3P_2$ transitions, than those of Jongerius. The percentage difference ranges from 4 to 65% and lies outside of the reproducibility limits placed on the separate measurements. The absolute measurements of Jongerius were carried out under conditions similar to those of the present investigation with only a slightly different calibration procedure. The origin of the discrepancy between the two sets of cross sections is still unclear.

V. OPTICAL EXCITATION FUNCTIONS

The general qualitative features of the excitation functions are now examined. The secondary lines will be discussed first, so that one may attempt to form conclusions concerning their general shape. This necessity arises because the upper levels contribute, by cascade transitions, to the population of the states of our primary interest. The information gained through this examination will be used in the interpretation of the excitation functions of the $6\,^3D_3$, $6\,^3D_2$, $7\,^3S_1$, and $7\,^1S_0$ levels.

A. Triplet *S* and *P* Levels

The excitation functions of the $n\,^3P_2$–$7\,^3S_1$($n=8$ to 14), $n\,^3P_{1,0}$–$7\,^3S_1$($n=9$ to 14), and $n\,^3S_1$–$6\,^1P_1$($n=8$

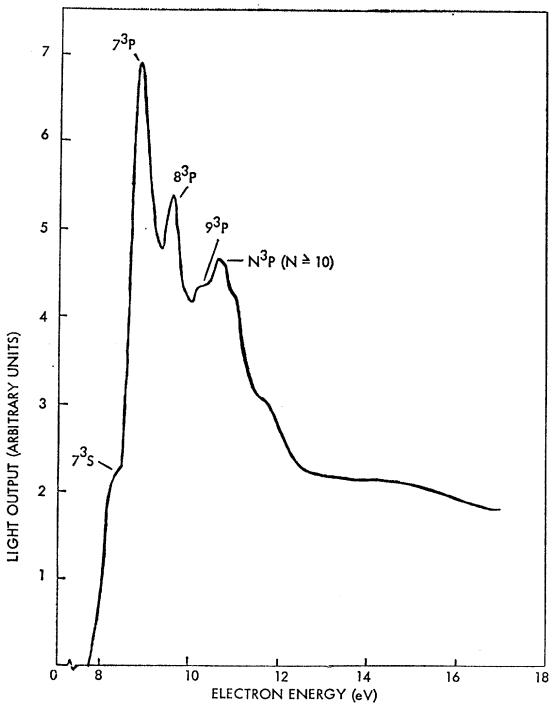

FIG. 6. $7\,^3S_1$–$6\,^3P_2$ optical excitation function shown on an expanded energy scale.

to 10) transitions have been measured. Excitation curves for the $8\,^3P_2$–$7\,^3S_1$ and $10\,^3P_2$–$7\,^3S_1$ lines are shown in Fig. 5. The $^3P_2$ states are selected for illustration because they are free from mixings with the singlet states. All these curves have the normal triplet characteristic, namely, they possess steep maxima near the onset voltage and experience a rapid decrease with increasing electron energy. The excitation function of the $8\,^3P_2$–$7\,^3S_1$ (6907 Å) transition exhibits fine structure occuring near its threshold. Two distinct peaks of comparable height, are resolved. It is believed that the initial peak is the result of the direct excitation of the $8\,^3P_2$ level, while the second is due to its population by cascade transitions from higher states. The excitation functions of all the other lines in the $n\,^3P_2$–$7\,^3S_1$ series have the same general features. Some of these curves, however, do not decay at high electron energies as rapidly as the ones shown in Fig. 5, possibly due to the unresolved adjacent lines.

Most of the lines of the $n\,^3P_1$–$7\,^3S_1$ family are not resolved from the corresponding members of $n\,^3P_0$–$7\,^3S_1$. With the exception of the case of $12\,^3P_1$, the excitation curves for these transitions are thoroughly distorted because of the presence of numerous unresolved Hg I and Hg II lines. The singlet-triplet mixing in the $n\,^3P_1$ further complicates the shape of the excitation functions. The $12\,^3P_1$–$7\,^3S_1$ (4992 Å) line, on the other hand, is not contaminated by any known Hg I and Hg II lines and its excitation function does experience a relatively sharp maximum near the threshold as shown in Fig. 5.

Of the three lines of the type $n\,^3S_1$–$6\,^1P_1$($n=8, 9, 10$) studied, only the $8\,^3S_1$ one was totally resolved from adjacent lines. The curve of the $8\,^3S_1$–$6\,^1P_1$ line (Fig. 5) exhibits the usual sharp peak near its onset, but the fast decay at higher electron voltage is missing. At this time no valid explanation can be suggested for this apparent flat appearance.

B. Singlet *S* and *P* Levels

The excitation functions of the $n\,^1P_1$–$7\,^3S_1$ and $n\,^1P_1$–$7\,^1S_0$ series should exhibit similar shapes since the transitions eminate from a common upper level. The curves representing the $8\,^1P_1$ and $9\,^1P_1$ levels do show reasonable agreement as may be seen in Fig. 5. The $8\,^1P_1$–$7\,^1S_0$ (6716 Å) and $8\,^1P_1$–$7\,^3S_1$ (6073 Å) lines are slightly distorted, respectively, by the 6715 and 6089-Å lines of Hg II. Likewise, the $9\,^1P_1$–$7\,^1S_0$ (6234 Å) and the $9\,^1P_1$–$7\,^3S_1$ (5676 Å) transitions are subject to the influence of the unresolved Hg I (6242 and 6220 Å) and Hg II (5677 Å) lines. Such distortion becomes more pronounced for the higher states and the resemblance between the two series is no longer apparent. The very broad maximum in these curves reminds one of a similar structure in the excitation functions of the ^1P states of helium.[1] The shallow peak near the onset may be attributed to cascade of the upper levels.

The two excitation functions for the $8\,^1S_0$ and $9\,^1S_0$ states exhibit sharp peaks in addition to broad maxima appearing at higher excitation voltages (Fig. 5). The $8\,^1S_0$–$6\,^1P_1$ transition is well isolated from the influence of all other spectral lines. It possesses two peaks at a sufficient energy above the threshold to suggest cascade transitions from the $8\,^3P_1$ and $n\,^3P_1$ ($n \geq 9$) levels. The broad maximum occurring at approximately 30 eV is attributed to the direct excitation of $8\,^1S_0$ and cascade from the $n\,^1P_1$ levels. There has been some disagreement in the literature as to the interpretation of these maxima in the excitation functions. Schaffernicht[22] ascribed the broad maximum to the direct-excitation process and the sharp peaks at lower energies to cascade. Zapesochny and Frisch,[23] however, suggested that the excitation functions for the singlet states possess a very steep peak near the onset voltage followed by a diffuse one at higher energy. More discussion about this point will be given in connection with the excitation functions of the primary lines. Although one cannot rule out the possibility of double-maximum curves for the ^1S states, there is insufficient experimental evidence for one to definitely associate the narrow peaks with direct excitation, since these peaks can be accounted for adequately by cascade processes.

C. *D* Levels

The $n\,^1D$–$6P$ lines are not resolved from the $n\,^3D$–$6P$ series; thus the excitation functions representing the combined transitions are observed. In Fig. 5 is included the curve for the $6\,^3D_1$–$6\,^1P_1$ and $6\,^1D_2$–$6\,^1P_1$ transitions.

All of the excitation functions for the nD states studied in this work (aside from $8D$, which is distorted by an intense Hg II lines at 3914 Å) exhibit maxima at approximately 15 to 20 eV and experience a gradual decrease thereafter. The broad maxima may be associated with the presence of the ^1D states in every curve.

D. The "Primary" Lines

The excitation function of the transition $7\,^3S_1$–$6\,^3P_2$ (5461 Å) exhibits fine structure occuring near its threshold, which is shown on an expanded energy scale in Fig. 6. The initial peak of the curve is ascribed to the direct excitation of the $7\,^3S_1$ level. This supposition follows from the fact that the incident electrons do not possess sufficient energy to excite the higher levels which would populate the $7\,^3S_1$ state by cascade. The second peak occurs at approximately 0.2 eV above the onset potential of the $7\,^3P$ levels. Similar energy relationships exist between the remaining peaks and the critical potentials of the higher triplet levels. In addition, one recalls that the ^3P excitation functions are characterized by steep peaks occuring within a few tenths of an electron volt of their onset. These facts suggest that the fine structure is the result of cascade transitions from the $n\,^3P$ levels as indicated in Fig. 6.

The optical-excitation function of the $7\,^1S_0$–$6\,^3P_1$ transition (Fig. 4) shows the broad maximum characteristic of the singlet states. The first sharp peak lies about 0.1 eV below the excitation threshold of $7\,^3P_1$, but one cannot discount the possibility of cascade from this level because the incident electrons have an energy distribution as large as 0.8 eV. The second and third sharp peaks occur at energies above the threshold values of $8\,^3P_1$ and $9\,^3P_1$ and therefore may be identified as cascade transitions from these levels. Frisch and Zapesochny,[23] however, proposed that the first narrow peak is due to direct excitation because it occurs below the electron energy corresponding to maximum excitation of the $7\,^3P_1$ state. This supposition would require that the singlet excitation functions possess both a steep and a diffuse maximum. However, the conclusion of Frisch and Zapesochny[23] was based on energy differences of 0.2–0.5 eV, against which one has to consider the energy distribution of the incident electrons (reported as ±0.25 eV), the uncertainty associated with adjusting the electron energy scale to make the experimental onset voltages coincide with the theoretical values, and the effects of space charge.[21] While the possibility of double-peak excitation functions do indeed exist, the experimental evidence contained in our work is not sufficient at this time to make a definite conclusion.

The excitation functions of the $6\,^3D_3$–$6\,^3P_2$ line shows the usual triplet characteristic since the $^3D_3$ states are not subject to singlet-triplet mixing. On the other hand, the wave function for the $6\,^3D_2$ state does contain a singlet component which manifests itself in the form of a broad maximum in the excitation function of the $6\,^3D_2$–$6\,^1P_1$ line.

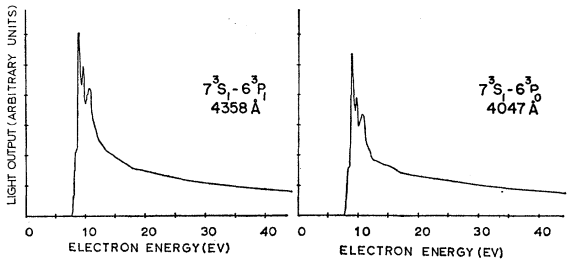

FIG. 7. Optical excitation functions of lines eminating from a common upper level.

VI. RELATIVE INTENSITIES

For the transitions originating from the same upper state, the relative intensities at a given electron energy depend only on the line strengths but not on the excitation cross section to the upper state of these transitions. Thus, it is instructive to compare the relative intensities of these lines measured in the excitation experiment with the theoretical values, before proceeding to the evaluation of the excitation cross sections. The most interesting group of these lines are the $7\,^3S_1$–$6\,^3P_{2,1,0}$ transitions (5461, 4358, 4047 Å). The shape of the excitation functions corresponding to the three transitions are observed to be similar. The curves representing the 4358- and 4047-Å lines are shown in Fig. 7. Under the framework of the theory presented in this paper, the relative intensities of these lines are completely determined by their frequencies, the appropriate Clebsch-Gordan coefficients, and the mixing coefficients. Particularly, the intensity ratio of the 5461- and 4047-Å lines is not even dependent upon the mixing coefficients, because the $6\,^3P_2$ and $6\,^3P_0$ do not mix with the singlet states. The observed intensity ratios for the 5461-, 4358-, and 4047-Å lines are 96±13:100:36±3, which differ appreciably from the theoretical values of 70:100:46. The mechanism of self-absorption was examined as a possible cause for distorting the experimental ratio. An estimate of the order of magnitude of this effect shows that it is too small to alter the intensity ratio. The observed linearity between the light output and density of atoms also suggests the nonimportance of the self-absorption process. The theoretical values are derived under the one-configuration approximation. Inclusion of configuration interaction in the wave function may change appreciably the theoretical intensities; however, a detailed calculation must be performed to estimate the magnitude of this effect. At present no definite explanation can be offered for this discrepancy.

Further studies have been carried out for the intensity ratios of spectral lines eminating from the $7\,^1S_0$ and $n\,^1P_1$ levels. The experimental values are compared to the theoretical intensity ratios which are dictated by

TABLE IV. Intensity ratios of lines originating from the $7\,^1S_0$ and $n\,^1P_1$ levels.

Transition	Wavelength (Å)	Intensity ratio Experiment	Intensity ratio Theory	Mixing coeff. (α^2/β^2)
$7\,^1S_0$–$6\,^1P_1$	10140	2.0	0.86	33
$7\,^1S_0$–$6\,^3P_1$	4078			
$8\,^1P_1$–$7\,^1S_0$	6716	1.5	1.7	2.8
$8\,^1P_1$–$7\,^3S_1$	6072			
$9\,^1P_1$–$7\,^1S_0$	6234	1.4	12	17
$9\,^1P_1$–$7\,^3S_1$	5676			
$10\,^1P_1$–$7\,^1S_0$	5803	0.59	7	10
$10\,^1P_1$–$7\,^3S_1$	5317			

the mixing coefficients (Table IV). Satisfactory agreement is found for the $8P$ level. In the case of the $7S$ state, the deviation is larger than what would be expected from the experimental uncertainty and the accuracy of the mixing coefficient. The value of β for the $9P$ and $10P$ which were obtained from the fine structure analysis with two parameters (K and λ) are seen to be surprisingly small. It is possible that the two-parameter theory of fine structure is not adequate for these high states and the errors of the mixing coefficients thus calculated may be responsible for the discrepancy between the theoretical and experimental intensity ratios.

VII. DIRECT-EXCITATION CROSS SECTIONS

The procedure for evaluating the direct-excitation cross sections from the experimental data has been given in detail in Ref. 1. The apparent excitation cross section $Q'(j)$ of the j state is related to the experimentally observed optical cross section $Q(j,k)$ of the $j \rightarrow k$ transition as

$$Q'(j)=Q(j,k)B(j,k), \tag{3}$$

where $B(j,k)$ is the branching ratio. Here we have neglected the polarization correction.[1] The direct-excitation cross section Q is obtained as

$$Q(j)=Q'(j)-\sum_{i>j} Q(i,j). \tag{4}$$

The last term in Eq. (4) represents the cascade from all the levels above j.

A. $7\,^1S_0$ State

The optical cross section of the $7\,^1S_0$–$6\,^3P_1$ transition is measured as $(1.3\pm0.15)\times10^{-18}$ cm^2 at 15 eV. Since the mixing coefficient β for the $(6s)(6p)$ configuration is small, the branching ratio for this intercombination line is very sensitive to the magnitude of this coefficient. Although the values of β determined from the g factor and lifetime data are very consistent with each other, an appreciable discrepancy is found between the theoretical and experimental values of the intensity ratio of the $7\,^1S_0$–$6\,^3P_1$ to $7\,^1S_0$–$6\,^1P_1$ lines (Table IV). This discrepancy suggests the possibility that the theoretical branching ratio $B(7\,^1S_0,6\,^3P_1)$ may depend quite strongly on the theoretical model of the atom employed for the calculation. Consequently, we have chosen the $7\,^1S_0$–$6\,^1P_1$ line to obtain $Q'(7\,^1S_0)=(9.4\pm1.9)\times10^{-18}$ cm^2. For this transition the experimental uncertainty is rather large, but the branching ratio does not change significantly with respect to variations of β. Hence the result of the apparent cross section should be less susceptible to the imperfections of the theory.

The cascade contribution from the $n\,^1P_1$ states with $n=8$ to 14 is determined from the measured cross sections. By extrapolation we obtain

$$\sum_{n\geq8} Q(n\,^1P_1,7\,^1S_0)=(1.8\pm0.4)\times10^{-18}\ \text{cm}^2.$$

No experimental data are available for $Q(7\,^1P_1,7\,^1S_0)$, thus this quantity has to be obtained from the extrapolation of the observed values of $Q(n\,^1P_1,7\,^1S_0)$. This procedure yields 2×10^{-18} cm^2 for the cascade contribution of the $7\,^1P_1$ level. The relation

$$Q(7\,^3P_1,7\,^1S_0) = Q(7\,^3P_1,7\,^3S_1)A(7\,^3P_1,7\,^1S_0)/A(7\,^3P_1,7\,^3S_1)$$

was used in conjunction with the extrapolated value $Q(7\,^3P_1,7\,^3S_1)\simeq7.2\times10^{-19}$ cm^2 and the transition probabilities listed in Table I to obtain the estimate $Q(7\,^3P_1,7\,^1S_0)\simeq1.4\times10^{-19}$ cm^2. Transition cross sections from other states of the $n\,^3P$ family are much smaller and will be neglected. Equation (4) then gives $Q(7\,^1S_0)=(5.5\pm2.6)\times10^{-18}$ cm^2. In this case the cascade from all of the upper states constitutes about 42% of the total population.

B. Analysis of the $7\,^3S_1$–$6\,^3P_2$ Data

The analysis of the excitation data of the $7\,^3S_1$–$6\,^3P_2$ line is especially interesting because it turns out that cascading from the $7\,^3P_2$ state is mainly responsible for the observed population of the $7\,^3S_1$ state, while direct excitation plays only a minor role. To demonstrate this, let us write

$$Q(7\,^3S_1)=Q'(7\,^3S_1)-\sum_{n\geq7} Q(nP,7\,^3S_1), \tag{5}$$

where $Q'(7\,^3S_1)$ is determined from the experimental data as $(1.8\pm0.2)\times10^{-17}$ cm^2 at 15 eV. We have also measured $Q(nP,7\,^3S_1)$ for $n=8$–14 with the exception of $Q(8\,^3P_1,7\,^3S_1)$ and $Q(8\,^3P_0,7\,^3S_1)$. The latter two cross sections are estimated from theoretical calculations as 5.7×10^{-20} and 8.2×10^{-20} cm^2, respectively. Cascade from states above $n=14$ can be obtained by extrapolation. This yields

$$\sum_{n\geq8} Q(nP,7\,^3S_1)\simeq(2.3\pm0.4)\times10^{-18}\ \text{cm}^2.$$

For the $7\,^1P_1$ and $7\,^3P_1$ states, extrapolation of the

experimental data gives 9.6×10^{-19} and 7.2×10^{-19} for $Q(7\,^1P_1,7\,^3S_1)$ and $Q(7\,^3P_1,7\,^3S_1)$, respectively. The $7\,^3P_2$ and $7\,^3P_0$ states, on the other hand, must be considered separately as they cascade entirely to $7\,^3S_1$ (the branching ratio being unity) and their cascade contributions are expected to be much larger than the ones estimated above. Equation (5) now becomes

$$Q(7\,^3S_1)=(1.4\pm0.3)\times10^{-17}\text{ cm}^2-Q'(7\,^3P_2)-Q'(7\,^2P_0). \tag{6}$$

Since the cross sections for S-P transitions are generally much larger than the corresponding S-S transitions, Eq. (5) shows that the major contribution to the population of the $7\,^3S_1$ state comes from the cascade terms of $7\,^3P_2$ and $7\,^3P_0$ rather than direct excitation. Theoretical calculations by Born-Oppenheimer approximation give 5.5×10^{-19} cm^2 for $Q(7\,^3S_1)$. If we accept this theoretical value as being a reasonable estimate, the direct-excitation term in Eq. (6) can be neglected. Furthermore, the Born-Oppenheimer theoretical cross section of the $7\,^3P_2$ state is five times larger than that of $7\,^3P_0$. This relationship results directly from the Clebsch-Gordan coefficients of the two states concerned. Therefore, one may expect that a more refined calculation would also yield $Q(7\,^3P_2)\gg Q(7\,^3P_0)$. Neglecting the latter in comparison with the former, we can finally obtain an estimate of $Q'(7\,^3P_2)$ at 15 eV as

$$Q'(7\,^3P_2)\sim1\times10^{-17}\text{ cm}^2.$$

It is rather interesting that the excitation data of the $7\,^3S_1$–$6\,^3P_2$ line should yield an estimate of the excitation cross section of the $7\,^3P_2$ state rather than the $7\,^3S_1$. Actually this conclusion can be anticipated from the shape of the excitation function of the 5461-Å line shown in Fig. 6. Here the second peak which occurs at the threshold energy of the $7\,^3P$ states does indeed overpower the first which corresponds to the direct excitation of the $7\,^3S_1$ state. We can equally well perform a similar analysis for the 4358 Å ($7\,^3S_1$–$6\,^3P_1$) and for the 4047 Å ($7\,^3S_1$–$6\,^3P_0$) lines. The values of $Q'(7\,^3S_1)$ determined by the three lines will differ from each other by about 30%, but the order of magnitude of the value of $Q'(7\,^3P_2)$ will not be altered.

C. $7\,^3P_2$ State

Direct measurements of the excitation cross section of the $7\,^3P_2$–$7\,^3S_1$ transition give $Q'(7\,^3P_2)=(2.5\pm0.8)\times10^{-17}$ cm^2, which is in reasonable agreement with the estimated value obtained in the Sec. VII.B. No transitions which terminate at the $7\,^3P_2$ state have been measured. However, the cascade population of this state is expected to account for only a small fraction of the observed value because the cross sections of the P states are generally much larger than those of the S and D states. Indeed, we estimate $Q(8\,^3S_1,7\,^3P_2)$ to be less than 4×10^{-21} cm^2. Likewise, our estimation shows that the cascade contribution from the $n\,^3D$ states are also entirely negligible.

Unlike the case of the 5461-Å line, the second peak of the optical excitation function of the $8\,^3P_2$–$7\,^3S_1$ transition (Fig. 5) is only slightly higher than the first. This feature supports our contention that for the $^3P_2$ states the cascade population is subordinate to the contribution of the direct excitation.

D. $6\,^3D_3$ and $6\,^3D_2$ States

The cross section for direct excitation to the $6\,^3D_3$ level is

$$Q(6\,^3D_3)=Q'(6\,^3D_3)-\sum_{n\geq8}Q(nP,6\,^3D_3),$$

and similarly for $6\,^3D_2$. Here we have neglected the cascade contribution from the F states since the excitation cross sections to these states are believed to be very small. The apparent cross sections of $6\,^3D_3$ and $6\,^3D_2$ were determined experimentally to be $(7.5\pm1.3)\times10^{-18}$ cm^2 and $(7.0\pm1.3)\times10^{-17}$ cm^2 at 15 eV. The cascade contribution of the nP levels was obtained by employing the relationship

$$Q(nP,6\,^3D_{3,2})=Q(nP,7\,^3S_1)A(nP,6\,^3D_{3,2})/A(nP,7\,^3S_1).$$

In this manner, the cascade contributions to the $6\,^3D_3$ and $6\,^3D_2$ levels were found to be 2×10^{-20} cm^2 and 4×10^{-18} cm^2, respectively. Therefore, the direct excitation cross section at 15 eV is $(7.5\pm1.3)\times10^{-18}$ cm^2 for the $6\,^3D_3$ state and $(6.6\pm1.4)\times10^{-17}$ cm^2 for $6\,^3D_2$.

VIII. DISCUSSION OF RESULTS

Although the electron excitation of mercury has been investigated in several laboratories over the past 30 years, this work represents the first attempt to analyze quantitatively the excitation data and to elucidate the direct excitation cross section. The results of this investigation have pointed out some difficulties of using the optical method to determine the direct excitation cross sections of the heavy atoms. The vast number of lines in the spectra of the neutral and the ionized atom makes it difficult to isolate all the lines which one wishes to study. Secondly, to determine the apparent excitation functions from the optical measurements, one must have recourse to the theoretical transition probabilities. This requires accurate wave functions of the excited states which are not generally available. These difficulties did not arise in the study of helium, but become more serious for the heavier atoms.

In spite of these limitations, the excitation experiments of mercury do offer some interesting features which are not found in the case of helium. The complex structure of the energy levels makes it possible to compare the excitation cross sections of several lines originating from the same upper level. Since the relative intensities depend only on the transition probabilities,

TABLE V. Comparison between the experimental and theoretical values of the direct-excitation cross sections at 15 eV (in units of 10^{-18} cm^2).

State	Experimental cross section	Theoretical cross section: Born and Born-Oppenheimer	Theoretical cross section: Ochkur
$7\,^1S_0$	5.5±2.6	106	
$6\,^3D_2$	66±14	25	
$6\,^3D_3$	7.5±1.3	8.)	1.7
$7\,^3P_2$	25±8	37	6.4

the excitation data may provide some information about the structure of the atoms.

From the excitation data of helium it was found that the excitation functions of the singlet states have a broad peak, whereas those of the triplet states are characterized by a sharp maximum near the onset. Of all the singlet states observed, the ^1P group shows a more diffuse maximum than the others. This trend holds for mercury to the extent that the Russell-Saunders coupling applies, i.e., the characteristic sharp peaks were observed for the $^3S_1$, $^3P_{2,0}$, $^3D_3$ states but obscured by the singlet-triplet mixing in the case of $^3P_1$ and $^3D_2$. The distortion of the excitation curves due to the contamination of other lines prevents one from investigating quantitatively the rate of decrease of the singlet cross sections at larger electron energies.[27]

Direct excitation cross sections for the $7\,^1S_0$, $7\,^3P_2$, $6\,^3D_3$, and $6\,^3D_2$ states were determined at 15 eV only. At higher energies, the cascade analysis becomes inaccurate because of the distortion of excitation functions by the presence of the adjacent lines. Below 15 eV, the excitation curves begin to rise rapidly with decreasing electron energy. Since the electron beam has an energy spread of about 0.6 eV, the observed cross sections represent weighted averages of the actual values and may be subject to considerable error. With direct-excitation cross sections available at just one electron energy, only a very limited comparison with theoretical calculations can be made. This is shown in Table V. The theoretical excitation cross section of the $7\,^1S_0$ level is about 20 times larger than the experimental value. Even in the extreme case of zero cascade, the maximum experimental value of the direct excitation cross section is equal to the apparent excitation cross section which is 9×10^{-18} cm^2. The discrepancy is therefore most likely due to the inaccuracy of the theoretical value, although one would normally expect the Born approximation to give cross sections of the correct order of magnitude for the singlet states. More accurate calculations of the excitation cross section of the $7\,^1S_0$ state are needed. Because the singlet component of the wave function is the major contributor to the excitation cross section of the $6\,^3D_2$ state, the latter depends quite strongly on the mixing coefficient β. Nevertheless, the observed cross section of the $6\,^3D_2$ state agrees reasonably well with theory. The agreements between the experimental and theoretical values of $Q(6\,^3D_3)$ and $Q(7\,^3P_2)$ are also regarded as reasonable in view of the uncertainty of the approximate methods used in the theoretical calculations. However, similar studies of the excitation cross sections at several higher electron energies must be made before one can arrive at more general conclusions as to the over-all agreement between theory and experiment.

[27] H. W. S. Massey and E. H. S. Burhop, *Electronic and Ionic Impact Phenomena* (Oxford University Press, London, 1956), p. 145.

ACKNOWLEDGMENTS

It is a pleasure to thank Dr. R. M. St. John for making his equipment available to us during the beginning phase of this work. We also wish to acknowledge the technical assistance of Robert L. Legan, J. Alan Payne, and Francis A. Sharpton in the design and construction of the apparatus.